Inorganic Chemistry
Article

Inorg. Chem. **2009**, *48*, 9271–9281 **9271**
DOI: 10.1021/ic901090p

Complex Superstructures of $Mo_2P_4O_{15}$

Sarah E. Lister, Ivana Radosavljević Evans, and John S. O. Evans*

Department of Chemistry, Durham University, South Road, Durham, DH1 3LE, United Kingdom

Received June 5, 2009

We report structural studies on $Mo_2P_4O_{15}$ over the temperature range 16−731 K, which show that it is considerably more complex than revealed by earlier work. Its low-temperature structure has lattice parameters a = 24.1134(6) Å, b = 19.5324(5) Å, c = 25.0854(6) Å, β = 100.015(1)°, and V = 11635.0(5) Å^3 at 120 K, containing 441 unique atoms in space group *Pn*, a remarkably high number for a material with such a simple composition. $Mo_2P_4O_{15}$ undergoes a structural phase transition at ∼520 K to a high-temperature phase in space group $P\bar{1}$, with lattice parameters a = 17.947(3) Å, b = 19.864(3) Å, c = 21.899(3) Å, α = 72.421(3)°, β = 78.174(4)°, γ = 68.315(4)°, and V = 6877.2(19) Å^3 at 573 K. The high-temperature structure, with 253 unique atoms, retains much of the low-temperature complexity.

Introduction

Framework inorganic materials made up of corner-sharing metal-centered tetrahedra or octahedra show a wealth of fascinating properties. Zeolites, for example, are of use for ion exchange, gas sorption, catalysis, and many other applications.[1] Nasicon ($Na_{1+x}Zr_2(PO_4)_{3-x}(SiO_4)_x$) and structurally related phases show high ionic conductivity, and their chemical flexibility has been exploited for radioisotope capture and storage.[2] Other framework oxides are of interest as intercalation hosts for rechargeable lithium batteries.[3−5] We have a particular interest in the unusual thermal expansion properties and phase transitions of framework structures.[6,7]

One way of categorizing these materials is by the ratio of tetrahedral (T) to octahedral (M) cation sites they contain. An all-tetrahedral corner-linked oxide would have formula TO_2 [$TO_{4/2}$] and is represented by the many polymorphs of SiO_2 and high silica zeolites, several of which show negative thermal expansion.[8,9] An all-octahedral framework would be MO_3 [$MO_{6/2}$], and NTE has again been reported in ReO_3.[10,11] Between these two extremes, we have the 2T:1M MT_2O_7 [$(MO_{6/3})(TO_{4/2})_2$] materials such as ZrP_2O_7 and ZrV_2O_7, the large family of 3T:2M $M_2T_3O_{12}$ [$(MO_{6/2})_2(TO_{4/2})_3$] materials, and 1T:1M materials such as $NbOPO_4$ [$(MO_{6/2})$-$(TO_{4/2})$].[12−18] Members of all of these families show negative thermal expansion. These examples all contain fully corner-linked polyhedra, and the requirement for T−O−T or M−O−M linkages within them varies systematically as the T/M ratio changes. For a stoichiometry of MT_2O_7, one has T_2O_7 units containing a T−O−T linkage, which in turn link to MO_6 octahedra. At 3T:2M (where 3×4 corners of a tetrahedron match 2×6 corners of an octahedron), neither T−O−T or M−O−M links are required, and beyond this limit, M−O−M links are needed. In addition to the many polyhedral arrangements possible within each such scheme, structural possibilities are widened further if one considers frameworks in which nonlinked corners are allowed. If, for example, we introduce an additional oxygen into the structure of cubic MT_2O_7 and allow one oxygen of each TO_4 to become one-coordinate, we obtain the structure of ZrW_2O_8, which can be described as corner-sharing ZrO_6 octahedra

*To whom correspondence should be addressed. E-mail: john.evans@durham.ac.uk.

(1) Wright, P. A. *Microporous Framework Solids*; RSC: Cambridge, U. K., 2008.
(2) Scheetz, B. E.; Agrawal, D. K.; Breval, E.; Roy, R. *Waste Manage.* **1994**, *14*, 498–505.
(3) Padhi, A. K.; Nanjundaswamy, K. S.; Goodenough, J. B. *J. Electrochem. Soc.* **1997**, *144*, 1188–1194.
(4) Tarascon, J. M.; Armand, M. *Nature* **2001**, *414*, 359–367.
(5) Armand, M.; Tarascon, J. M. *Nature* **2008**, *451*, 652–657.
(6) Evans, J. S. O. *J. Chem. Soc., Dalton Trans.* **1999**, *19*, 3317–3326.
(7) Stinton, G. W.; Hampson, M. R.; Evans, J. S. O. *Inorg. Chem.* **2006**, *45*, 4352–4358.
(8) Barrera, G. D.; Bruno, J. A. O.; Barron, T. H. K.; Allan, N. L. *J. Phys.: Condens. Matter* **2005**, *17*, R217–R252.
(9) Colligan, M.; Forster, P. M.; Cheetham, A. K.; Lee, Y.; Vogt, T.; Hriljac, J. A. *J. Am. Chem. Soc.* **2004**, *126*, 12015–12022.
(10) Dapiaggi, M.; Fitch, A. N. *J. Appl. Crystallogr.* **2009**, *42*, 253–258.
(11) Chatterji, T.; Henry, P. F.; Mittal, R.; Chaplot, S. L. *Phys. Rev. B* **2008**, *78*, 134105.
(12) Khosrovani, N.; Korthuis, V.; Sleight, A. W.; Vogt, T. *Inorg. Chem.* **1996**, *35*, 485.
(13) Khosrovani, N.; Sleight, A. W.; Vogt, T. *J. Solid State Chem.* **1997**, *132*, 355–360.
(14) Korthuis, V.; Khosrovani, N.; Sleight, A. W.; Roberts, N.; Dupree, R.; Warren, W. W. *Chem. Mater.* **1995**, *7*, 412–417.
(15) Evans, J. S. O.; Mary, T. A.; Sleight, A. W. *J. Solid State Chem.* **1997**, *133*, 580.
(16) Sleight, A. W.; Brixner, L. H. *J. Solid State Chem.* **1973**, *7*, 172.
(17) Amos, T. G.; Sleight, A. W. *J. Solid State Chem.* **2001**, *160*, 230–238.
(18) Amos, T. G.; Yokochi, A.; Sleight, A. W. *J. Solid State Chem.* **1998**, *14*, 303–307.

Published on Web 09/10/2009

and WO_4 tetrahedra, with one oxygen per WO_4 tetrahedron being formally one-coordinate. This family shows a wealth of fascinating properties related to its unusual topology.[19−28]

In this paper, we report structural studies on the Mo(V)-containing material $Mo_2P_4O_{15}$ ($MoP_2O_{7.5}$), which again has a stoichiometry related to cubic MP_2O_7 phases but now contains 0.5 extra oxygen atoms per formula unit. Its composition is thus midway between MT_2O_7 and MT_2O_8 materials. The Mo(V) valence state has been confirmed by electron paramagnetic resonance.[29] There have been a number of structural studies on this phase, and the basic polyhedral connectivity is well established.[30−33] The structure contains MoO_6 octahedra and PO_4 tetrahedra with tetrahedra corner-linked to form P_4O_{13} groups (Figure 1). These contain three "bridging" P−O−P oxygens, and the remaining 10 are shared with Mo sites. The MoO_6 octahedra are completed by a one-coordinate or "terminal" oxygen, Figure 1, such that the formula is perhaps better expressed as $(MoO)_2P_4O_{13}$. In contrast to ZrW_2O_8, the one-coordinate oxygen is located on the octahedral rather than the tetrahedral atom.

While this basic connectivity is well established, there has been some debate about the precise details of the structure. Unit-cell parameters that have been reported to date are summarized in Table 1. The various cells are clearly closely related, with each volume a simple multiple of the smallest cell (hereafter, the $P2_1/c$ subcell) used by Costentin et al. In the Costentin et al. publication, analysis of single-crystal data gave R/R_w values of 3.6/3.7% using a simple model containing 11 atoms in the asymmetric unit, though it was necessary to disorder the central P−O−P bridging oxygen atom of P_4O_{13} groups over two sites close to a center of inversion to achieve this fit, and the authors acknowledged that anisotropic displacement parameters (adp's) were unusually large.

We have previously reported the structure of this material at 120 K.[33] In this paper, we report structural studies on $Mo_2P_4O_{15}$ over a temperature range of 16−731 K which reveal that it is considerably more complex than suggested by earlier work over this entire range. Its low-temperature structure contains 441 atoms in the asymmetric unit, a remarkably high number for a material with such a simple composition. $Mo_2P_4O_{15}$ undergoes a structural phase transition at ∼520 K, but its high-temperature structure retains much of the low-temperature complexity.

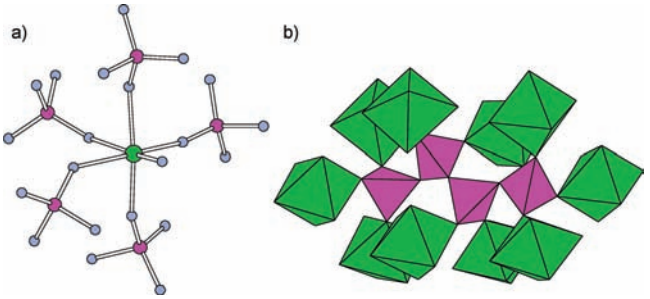

Figure 1. Portions of the structure of $Mo_2P_4O_{15}$ (a) emphasizing the local environment around each MoO_6 octahedron and (b) a P_4O_{13} unit made from corner-sharing PO_4 groups.

Experimental Section

$Mo_2P_4O_{15}$ was prepared following the method of Lezama et al.[29] A total of 1.4395 g of MoO_3 (10 mmol, Alfa, 99.95%) was intimately mixed with $(NH_4)_2HPO_4$ (30 mmol, Aldrich, 98+ %) and warmed at 5 K min^{-1} to 523 K, held at this temperature for 2 h, heated at 2 K min^{-1} to 873 K, held at this temperature for 6 h, and then cooled by turning off the furnace. The resulting green solid was washed with demineralized water and dried to produce 2.1981 g (79% yield) of $Mo_2P_4O_{15}$ (PDF 76-2079) containing a number of crystals of suitable size for single-crystal experiments.

High-temperature powder diffraction experiments were performed using Cu $K\alpha_1$ radiation on a Bruker d8 diffractometer equipped with a Ge(111) incident beam monochromator, a Vantec psd, and an Anton Paar HTK1200 heating stage using a sample mounted on an amorphous silica disk. To check temperature calibration, the sample was mixed with an Al_2O_3 internal standard.[34] A total of 309 30-min scans from 10 to 90° 2θ with a step size of 0.017° 2θ were recorded in 5 K steps from 308 to 731 K in two cycles of heating and cooling. Excellent reproducibility was obtained between cycles. Low-temperature experiments were performed using $K\alpha_1$/$K\alpha_2$ radiation on a Bruker d8 diffractometer equipped with a Lynxeye psd and an Oxford Cryosystems pHeniX cryostat. The sample was mixed with a Si internal standard and sprinkled on an Al plate. Peak positions of both Si and Al were used to verify temperature calibration.[34] Data sets were collected from 10 to 90° 2θ in step sizes of 0.017° 2θ over 20 min time slices as the sample was cooled at 17 K hr^{-1} from 300 to 16.4 K then warmed from 16.4 to 300 K.

Powder diffraction data were analyzed using a combination of Rietveld and Pawley refinements to extract the temperature dependence of cell parameters. For high-temperature refinements, a total of 67 parameters were refined for each data set (4 cell parameters, 24 terms of a spherical harmonic preferred orientation correction, 3 adp's, 4 peak shape parameters, and a scale factor for $Mo_2P_4O_{15}$; 2 cell parameters, 2 atomic coordinates, 2 adp's, 4 peak shape parameters, and a scale factor for the Al_2O_3 standard; 18 background parameters, a sample height correction, and 1 parameter to describe axial divergence). For low-temperature data, 74 parameters were refined (4 cell parameters, 24 terms of a spherical harmonic preferred orientation correction, 3 adp's, 6 peak shape parameters, and a scale factor for $Mo_2P_4O_{15}$; 1 cell parameter, 1 adp, 6 peak shape parameters,

(19) Mary, T. A.; Evans, J. S. O.; Vogt, T.; Sleight, A. W. *Science* **1996**, *272*, 90–92.
(20) Ernst, G.; Broholm, C.; Kowach, G. R.; Ramirez, A. P. *Nature* **1998**, *396*, 147.
(21) Ramirez, A. P.; Kowach, G. R. *Phys. Rev. Lett.* **1998**, *80*, 4903.
(22) Perottoni, C.; da Jornada, J. A. H. *Science* **1998**, *280*, 886–889.
(23) Hancock, J. N.; Turpen, C.; Schlesinger, Z.; Kowach, G. R.; Ramirez, A. P. *Phys. Rev. Lett.* **2004**, *93*, 225501.
(24) Drymiotis, F. R.; Ledbetter, H.; Betts, J. B.; Kimura, T.; Lashley, J. C.; Migliori, A.; Ramirez, A. P.; Kowach, G. R.; Van Duijn, J. *Phys. Rev. Lett.* **2004**, *93*, 025502.
(25) Kennedy, C. A.; White, M. A. *Solid State Commun.* **2005**, *134*, 271–276.
(26) Pantea, C.; Migliori, A.; Littlewood, P. B.; Zhao, Y.; Ledbetter, H.; Lashley, J. C.; Kimura, T.; Van Duijn, J.; Kowach, G. R. *Phys. Rev. B* **2006**, *73*, 214118.
(27) Keen, D. A.; Goodwin, A. L.; Tucker, M. G.; Dove, M. T.; Evans, J. S. O.; Crichton, W. A.; Brunelli, M. *Phys. Rev. Lett.* **2007**, *98*, 225501.
(28) Dubbeldam, D.; Walton, K. S.; Ellis, D. E.; Snurr, R. Q. *Angew. Chem., Int. Ed.* **2007**, *46*, 4496–4499.
(29) Lezama, L.; Rojo, J. M.; Pizarro, J. L.; Arriortua, M. I.; Rojo, T. *Solid State Ionics* **1993**, *63−65*, 657.
(30) Schulz, I. *Z. Anorg. Allg. Chem.* **1955**, *281*, 99–112.
(31) Minacheva, L. K.; Antsyshkina, A. S.; Lavrov, A. V.; Sakharova, V. G.; Nilolaev, V. P.; Porai-Koshits, M. A. *Rus. J. Inorg. Chem.* **1979**, *24*, 51–53.
(32) Costentin, G.; Leclaire, A.; Borel, M.-M.; Grandin, A.; Raveau, B. *Z. Kristallogr.* **1992**, *201*, 53–58.
(33) Lister, S. E.; Evans, I. R.; Howard, J. A. K.; Coelho, A. A.; Evans, J. S. O. *Chem. Commun.* **2004**, *22*, 2540–2541.
(34) Stinton, G. W.; Evans, J. S. O. *J. Appl. Crystallogr.* **2008**, *40*, 87–95.

Table 1. Unit Cell Parameters and Space Groups Previously Reported for $Mo_2P_4O_{15}$ at Room Temperature and below[a]

reference	space group	a/Å	b/Å	c/Å	β/°	V/Å^3	V/V_{sub}
Schulz[30]	–	≈16.7	≈19.3	≈10.8	≈107.5	≈3320	6
Minacheva et al.[31]	*Pc*	8.288(2)	19.529(5)	10.690(3)	106.7(3)	1657.18	3
Costentin et al.[32]	$P2_1/c$	8.3068(8)	6.5262(6)	10.7181(11)	106.7050(78)	556(1)	1
this work[33]	*Pn*	24.133(2)	19.579(2)	25.109(2)	99.962(3)	11685(1)	21

[a] V_{sub} refers to the volume of the cell reported by Costentin.

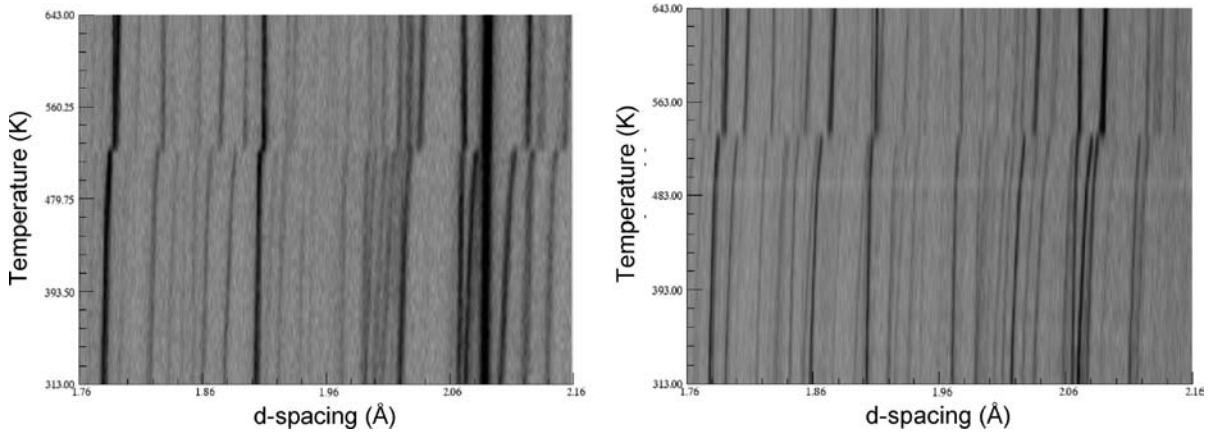

Figure 2. X-ray and neutron diffraction data showing the phase transition in $Mo_2P_4O_{15}$. Data presented as a pseudo-film plot using Powder 3D software.[39] The light band in the neutron data is caused by a shorter effective collection time at this temperature.

and a scale factor for Si; 1 cell parameter, 5 peak intensities, a height offset parameter, and 6 peak shape parameters for Al; 12 background parameters, a sample height correction, and 1 parameter to describe axial divergence). $Mo_2P_4O_{15}$ and Si were modeled using the Rietveld method, whereas the textured Al sample holder was fitted using the Pawley method. These protocols gave excellent fits to data over the whole temperature range, and checks were made to ensure that other parameters did not correlate significantly with the key unit-cell parameters we were trying to extract. All refinements were performed using the Topas Academic software suite controlled by local routines.[35]

Neutron powder diffraction experiments were performed using the HRPD diffractometer at the ISIS facility of the Rutherford Appleton Laboratory on a 6.03 g sample mounted in a 15 mm V can filled to a depth of 30 mm. Eight batches of material were combined to make this neutron sample. Data were collected over a time-of-flight range of 10−210 ms from 303 to 653 K in 10 K steps collecting 4 μAh (15 min) at each temperature. Due to a problem with detector electronics, data between 493 and 543 K were not fully recorded. When the sample reached 543 K, it was therefore recooled to 503 K, and data collection resumed. The effective data collection time at 493 K was therefore considerably shorter, and a small discontinuity is observed in the data which is not an intrinsic property of the sample.

The 120 and 293 K single crystal experiments were performed using a Bruker AXS Smart 6000 diffractometer with Mo Kα_1 radiation. Temperature control was achieved using an Oxford Cryosystems cryostream. A total of 4140 frames were collected in ω steps of 0.3° using a data collection time of 30 s and integrated using the SAINT software package.[36] Data were collected at generator settings of 35 kV and 50 mA to avoid problems with $\lambda/2$ contamination and corrected for absorption using the SADABS program.[37] Structure solution using simulated annealing methodologies was performed using the Topas Academic software suite[35] and final refinement using Crystals.[38] A second 293 K and 573 and 653 K data collections used an Enraf Nonius FR559 Crystal Heater. The heater attachment was mounted vertically on the diffractometer ($\chi = 0$). A total of 600 frames were collected in ω steps of 0.3° using a data collection time of 10 s. A total of 20 209 reflections with $I > 3\sigma(I)$ could be collected at 293 K using this configuration. No absorption correction was applied for data collected in this mode due to low redundancy. We note that successful refinement of the 293 K data led to verification of the use of this data collection strategy at high temperatures. Fewer reflections recorded at high temperatures (573 K, 7680 reflections; 653 K, 4834 reflections) led to higher standard uncertainties on refined values.

A sample of $Mo_2P_4O_{15}$ was examined using DSC, heating and cooling over the range 298−573 at 10 K/min, using a Perkin-Elmer Pyris 1 Differential Scanning Calorimeter.

Results

Thermal Expansion of $Mo_2P_4O_{15}$. Variable-temperature powder X-ray diffraction data were collected on a phase-pure sample of $Mo_2P_4O_{15}$ from 16.4 to 731 K. Data collected above room temperature are included in Figure 2. Unit-cell parameters were extracted by Rietveld refinement and sample temperatures calibrated using internal standards. The supercell model was used to fit all experimental data to allow volume evolution to be followed over the whole temperature range of cells; the

(35) Coelho, A. A. *TOPAS Academic: General Profile and Structure Analysis Software for Powder Diffraction Data*; Bruker AXS: Karlsruhe, Germany, 2004.

(36) *SAINT*, V6.02; Bruker AXS: Madison, WI, 2005.

(37) Sheldrick, G. M. *SADABS*; University of Göttingen: Göttingen, Germany, 1996.

(38) Betteridge, P. W.; Carruthers, J. R.; Cooper, R. I.; Prout, K.; Watkin, D. J. *J. Appl. Crystallogr.* **2003**, *36*, 1487.

(39) Hinrichsen, B.; Dinnebier, R. E.; Jansen, M. *Powder 3D*, v1.1; Stuttgart, Germany, 2004.

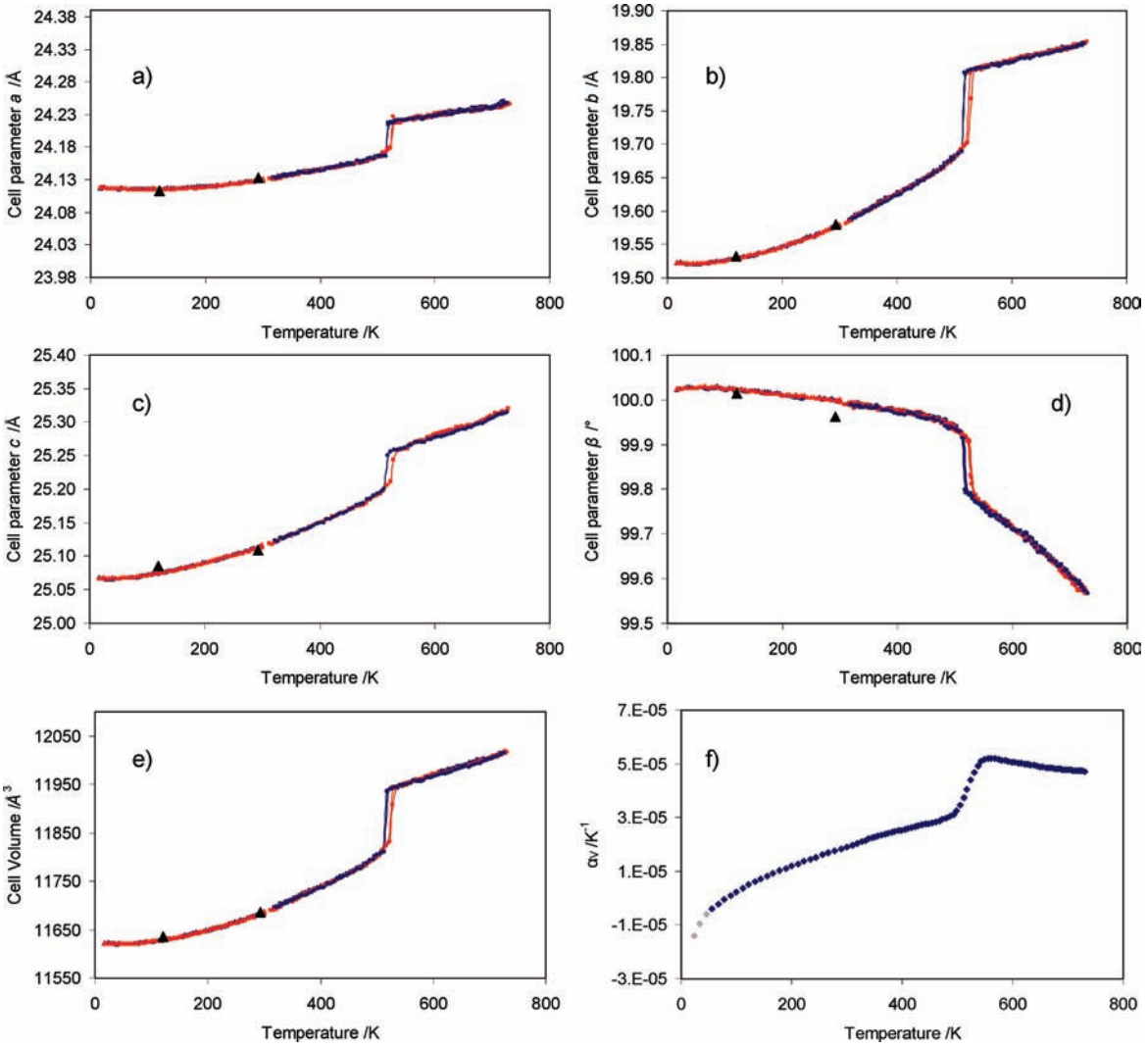

Figure 3. Temperature evolution of unit-cell parameters *a*, *b*, *c*, and β and volume and volume thermal expansion coefficients for the *Pn* supercell model. Legend (a−e): (red/blue ▲) low-temperature heating/cooling cycles, (red/blue ■) furnace heating/cooling cycle 1, (red/blue ●) furnace heating/cooling cycle 2, (black ▲) single-crystal data collections; (f) (blue/gray ♦) thermal expansion data.

cell volume plotted above ~ 520 K is therefore 1.75 times the true volume. The temperature dependence of unit-cell parameters *a*, *b*, *c*, β, and *V* are shown in Figure 3. Cell parameters derived from single-crystal experiments are included in Figure 3a−e for comparison and show good agreement with powder values. The temperature dependence of the volume thermal expansion coefficient (Figure 3f) was determined by fitting a Bezier function to the cell volume data followed by numerical differentiation. This procedure means the first few data points are relatively unreliable, but they are included in the figure in gray scale for completeness.

Figure 3f shows that $Mo_2P_4O_{15}$ displays negative thermal expansion below ~80 K. This is presumably due to population of negative-Gruneisen-parameter phonon modes at low temperatures involving local transverse vibrations of two-coordinate oxygen, as observed in other NTE framework structures. Above ~80 K, smooth positive expansion of all cell parameters is observed up to a sharp discontinuity in values at ~520 K, consistent with a first-order phase transition involving a volume change of $\Delta V \sim +1\%$. An approximately 10 K hysteresis in phase transition temperature is observed on cooling. Percentage changes in *a*, *b*, and *c* over the whole temperature range of +0.58, +1.68, and +1.0% are observed. Similar phase transition temperatures of 540 and 523 K on warming and cooling were obtained by differential scanning calorimetry; these data are included in the Supporting Information, Figure S1. Powder diffraction data recorded above and below the phase transition temperature showed relatively minor changes in the X-ray data but more marked changes in the intensities of the neutron data (Figure 2), suggesting that the changes occurring are displacive in nature and mainly affect the oxygen atoms. Despite the simplification of neutron diffraction data at high temperatures (in that fewer superstructure reflections are observed), reflections are still present which cannot be indexed using the $P2_1/c$ subcell.

Low-Temperature Structures of $Mo_2P_4O_{15}$. We have briefly reported the low-temperature structure of $Mo_2P_4O_{15}$ (hereafter referred to as α-$Mo_2P_4O_{15}$ or the *Pn* structure) in an earlier communication.[33] Diffraction images recorded at 120 K required a unit cell considerably larger than the 556 $Å^3$ monoclinic cell reported by Costentin et al.

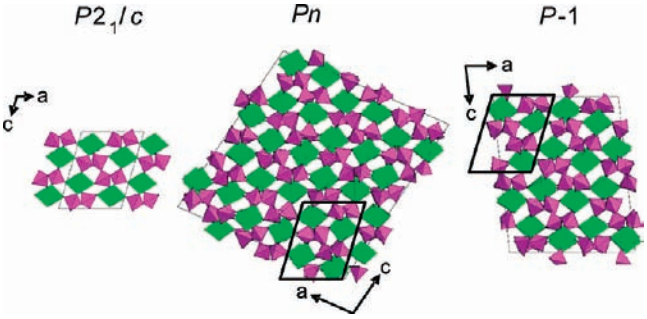

Figure 4. Comparison of the Costentin $P2_1/c$ model with Pn and $P\bar{1}$ structures of $Mo_2P_4O_{15}$. All structures viewed down the b axis. Pn and $P\bar{1}$ structures have b axes 3 times that of the Costentin model.

but could instead be indexed using a monoclinic cell with a = 24.133 Å, b = 19.579 Å, c = 25.109 Å, and β = 99.962°. The unit-cell volume (11685 Å^3) is 21 times that of the smaller cell, and the two cells can be related by the transformation (3 0 1, 0 3 0, −1 0 2), as shown in Figure 4. An automated analysis of systematic absences suggested space group $P2_1/n$, though careful inspection showed that reflections forbidden by the 2_1 axis were present though weak. The strongest $0\,k\,0$ reflection with $k \neq 2n$ was 0 7 0 with I = 1.54(3), which ranked 13352th of the observed reflections ordered by intensity, and was 0.02% of the strongest reflection [I = 9300(120)]. The cell volume and symmetry imply 441 atoms in the asymmetric unit.

Due to the significant pseudosymmetry present, the superstructure was initially solved using a simulated annealing methodology in the Topas software suite. Coordinates in the large cell were generated from those reported in the Costentin paper, and all atomic coordinates and a single overall temperature factor were allowed to refine to convergence from their ideal starting values using a limited data range ($< 25°$ 2θ). Soft restraints on Mo−O and P−O bond lengths were applied to retain a sensible connectivity. Since $Mo(V)O_6$ octahedra are known to be distorted,[40] restraints were only applied if bond lengths differed from expected values by > 0.4 Å. On convergence, atomic coordinates were reset to values randomly displaced from "ideal" positions by up to 0.1 Å and the structure re-refined. The best solution after several rounds of refinement/perturbation gave good agreement with the diffraction data. Isotropic refinement using the whole data set led to a final R factor of 3.49% for 43 738 reflections with $I > 3\sigma(I)$. Scatter plots of I_{obs} versus I_{calcd} showed no systematic deviations for weak reflections. We note that recently developed charge flipping methods of structure solution are particularly tolerant of pseudosymmetry.[41,42] In fact, a "default" application of charge flipping as implemented in the Topas software suite[43] will typically correctly locate all (or the vast majority of) atomic positions within a few seconds, producing a trial structure which can be refined readily. This procedure was therefore adopted for later high-temperature data sets.

Histograms of bond distances for the 42 crystallographically unique MoO_6 octahedra, 84 unique PO_4 tetrahedra, and P−O−P bridging bond angles in the structure are shown in Figure 5 alongside equivalent plots for the high-temperature structure. These will be discussed below. Data were also collected at 293 K in two separate experiments: one repeating the 120 K data collection strategy, and one using the setup employed for collections above room temperature. Correlation of bond distances and angles in the 120 and 293 K structures showed no significant changes over this temperature range, with similar spreads of bond distances and angles. The 293 K structures using the two strategies showed minimal differences.

High-Temperature Structures of $Mo_2P_4O_{15}$. High-temperature data were recorded using an Enraf Nonius heater attachment mounted on a Bruker AXS Smart 6000 at set temperatures of 573 and 653 K. Temperature calibration was checked both using an external thermocouple and by comparing unit-cell parameters to those obtained by powder diffraction methods; temperatures are estimated to be correct to ±10 K. While considerably fewer reflections were observed above the 520 K phase transition than below, significantly more reflections than those predicted by the 556 Å^3 subcell were observed. This is consistent with neutron powder diffraction data, which also showed extra reflections. Diffraction data at both 573 and 653 K could be indexed with a triclinic cell with a volume ~12 times that of the subcell (or 4/7 that of the true low-temperature cell), with 573 K values of a = 17.947 Å, b = 19.864 Å, c = 21.899 Å, α = 72.421°, β = 78.174°, γ = 68.315°, and V = 6877 Å^3. This can be related to the $P2_1/c$ subcell by the transformation matrix (−2 1 0, 0 3 0, −1 1 −2). The cell size and symmetry again imply a complex structure which would require 24 Mo, 48 P, and 181 O atoms (assuming, see below, that two oxygens lie on $\bar{1}$ sites) or 253 atoms in total in the asymmetric unit.

The structure of the high-temperature form (β-$Mo_2P_4O_{15}$) was solved using charge-flipping methods using an applied symmetry of $P\bar{1}$ and applying the tangent formula for phase refinement as described by Coelho.[44] This procedure successfully located all Mo and P sites and the majority of the 181 oxygens. The remainder were located using Fourier methods. A model with the same connectivity as at low temperatures resulted, which could be refined to R/R_w = 5.64/10.02% for 7680 observations with $I > 2\sigma(I)$. The parameter/observation ratio (1011:7680) restricts us to using isotropic displacement parameters. The structure was essentially unchanged at 653 K. Details of this refinement are given in Table 2, and the CIF is included in the Supporting Information.

Examination of histograms of bond distances and angles revealed a significant increase in spread relative to 120 or 293 K refinements, though mean values (Table 3) were within a standard uncertainty of those at lower temperatures. The lack of significant thermal expansion of bonds is a common observation in framework oxides and reflects the artificial reduction in bond lengths due to correlated

(40) Costentin, G.; Leclaire, A.; Borel, M. M.; Grandin, A.; Raveau, B. *Rev. Inorg. Chem.* **1993**, *13*, 77–101.
(41) Oszlányi, G.; Sütö, A. *Acta Crystallogr., Sect. A* **2004**, *60*, 134–141.
(42) Oszlanyi, G.; Suto, A.; Czugler, M.; Parkanyi, L. *J. Am. Chem. Soc.* **2006**, *128*, 8392–8393.
(43) Coelho, A. A. *Technical Reference, Topas Manual*, v4.1; Coelho Software: Brisbane, Australia, 2007.
(44) Coelho, A. A. *Acta Crystallogr., Sect. A* **2007**, *63*, 400–406.

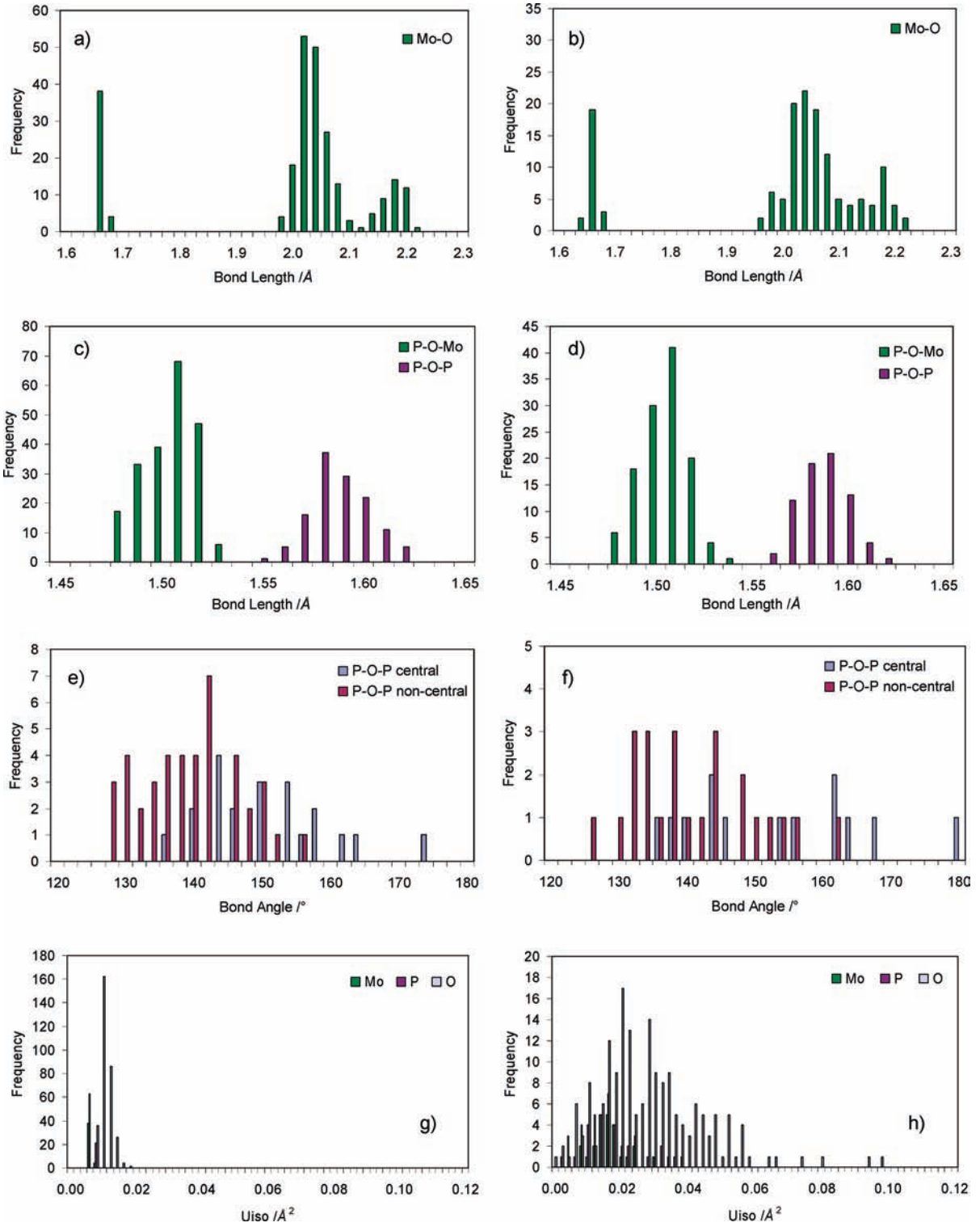

Figure 5. Histograms showing distributions of Mo−O (a,b) and P−O (c,d) bond lengths, P−O−P bond angles (e,f), and isotropic adp's (g,h) in 120 K (left column) and 573 K (right column) temperature forms of $Mo_2P_4O_{15}$. The *y* axes scales for histograms a−f reflect the 7:4 volume ratio between the two structures.

local motion compensating real expansion. The increased spread of distances is unsurprising given the significant reduction in the number of observed reflections and the higher parameter/observation ratio. For final refinements, bond distances within polyhedra were therefore restrained to values obtained at 120 K, with different values for "long", "medium", and "short" bonds within MoO_6 octahedra and for P−O(−Mo) and P−O(−P) P−O bonds. Restraints were weighted according to the standard deviations of the 120 K distributions. Refinement led to final *R* factors of $R/R_w = 6.15/10.73\%$, only marginally higher than those for the unrestrained model. Histograms of bond distances and angles are included in Figure 5 for comparison with the low-temperature structure.

Table 2. Crystallographic Data for the Superstructure Phases of $Mo_2P_4O_{15}$ Discussed in This Paper

	120 K	293 K	293 K (hothead)	573 K (restrained)	653 K (restrained)
chemical formula	$Mo_2P_4O_{15}$	$Mo_2P_4O_{15}$	$Mo_2P_4O_{15}$	$Mo_2P_4O_{15}$	$Mo_2P_4O_{15}$
M_r	555.77	555.77	555.77	555.77	555.77
cryst syst	monoclinic	monoclinic	monoclinic	triclinic	triclinic
space group (No.)	$P1n1$ (No. 7)	$P1n1$ (No. 7)	$P1n1$ (No. 7)	$P\bar{1}$ (No. 2)	$P\bar{1}$ (No. 2)
temp/K	120	293	293	573	653
a/Å	24.1134 (6)	24.133 (2)	24.1291 (10)	17.947 (3)	18.001(17)
b/Å	19.5324 (5)	19.5793 (18)	19.5817 (8)	19.864 (3)	19.98(3)
c/Å	25.0854 (6)	25.109 (2)	25.1108 (10)	21.899 (3)	22.00(3)
α/°	90	90	90	72.421 (3)	72.19(5)
β/°	100.0150 (10)	99.962 (3)	99.9780 (10)	78.174 (4)	78.24(6)
γ/°	90	90	90	68.315 (4)	68.42(4)
V/Å^3	11635.0 (5)	11685.4 (19)	11685.1 (8)	6877.2 (19)	6967(16)
Z	21	21	21	12	12
D_{calcd}/g cm^{-3}	3.331	3.317	3.317	3.220	3.179
λ/Å	0.71073	0.71073	0.71073	0.71073	0.71073
μ/mm^{-1}	2.93	2.92	2.92	2.84	2.80
no. of measured, independent, and obsd reflns	93645, 48060, 43783	216594, 48901, 9315	44022, 30516, 20209	25767, 25767, 7680	26002, 26002, 4834
criterion for obsd reflns	$I > 3.0\sigma(I)$	$I > 3.0\sigma(I)$	$I > 3.0\sigma(I)$	$I > 2.0\sigma(I)$	$I > 3.0\sigma(I)$
$R(F^2)$,[a] $R_w(F^2)$,[b] S	0.035, 0.060, 0.86	0.033, 0.083, 0.79	0.048, 0.115, 0.99	0.061, 0.107, 1.12	0.050, 0.128, 1.07
no. of params	1766	1766	1766	1011	1011
observations: parameters ratio	24.8	5.3	11.4	7.6	4.78

[a] $R = \sum||F_o| - |F_c||/\sum|F_o|$. [b] $R_w = [\sum||F_o^2| - |F_c^2||^2/\sum w|F_c^2|^2]^{1/2}$.

Table 3. Average Mo−O and P−O Bond Lengths in Refinements Discussed[a]

	120 K	293 K	293 K (hothead)	573 K free	573 K restrained
Mo−O (short)	1.653(5)	1.652(26)	1.647(11)	1.654(100)	1.652(9)
Mo−O (medium)	2.025(25)	2.025(35)	2.022(26)	2.041(94)	2.035(36)
Mo−O (long)	2.167(22)	2.172(35)	2.168(26)	2.171(89)	2.165(24)
P−O(−Mo)	1.500(13)	1.497(39)	1.497(16)	1.499(83)	1.502(14)
P−O(−P)	1.583(14)	1.583(36)	1.580(18)	1.582(91)	1.580(16)

[a] 293 K (hothead) refers to a 293 K refinement using the same data collection strategy used at 573 and 653 K. Numbers in parentheses are standard deviations of the set of individual distances in each category.

The unit cell size and space-group symmetry of β-$Mo_2P_4O_{15}$ require that two oxygen atoms lie on a center of inversion—those labeled O206 and O212. This implies that two P−O−P angles out of 36 in the structure are required to be 180° or that two of the 12 independent P_4O_{13} groups have an unfavorable local geometry. Figure 6 shows isotropic displacement parameters for central P_2O_7 units within these two P_4O_{13} groups and Fourier maps calculated in an O−P−O−P−O plane; these suggest that the behavior of these two oxygens differ. O212 appears to be best described as being disordered over two sites close to the inversion center, whereas O206 appears adequately described as lying on the inversion center with thermal displacement around this position. The O212 site was therefore split in final refinements, and the local P−O−P angle derived was ≈ 137°. An angle close to 180° for O206 is not unreasonable given the P−O−P angle distribution observed at low temperatures (Figures 5 and 7).

Discussion

Examination of the histograms of bond distances at 120 K in Figure 5 suggests a high-quality refinement. Given the connectivity of the polyhedra, one would expect that the 42 crystallographically unique MoO_6 octahedra would contain 42 "short" bonds to a terminal oxygen, 168 "medium" bonds to equatorial oxygens, and 42 "long" bonds to the oxygen trans to the terminal one. The histogram shows precisely this distribution. Similarly for the 84 PO_4 tetrahedra making up P_4O_{13} groups, one would expect 210 P−O(−Mo) bonds around 1.50 Å and 126 longer P−O(−P) bonds around 1.58 Å—exactly this distribution is again observed. Average bond lengths and their standard deviations are included in Table 3. Bond valence sums for all Mo and P sites deviate by < 0.16 units from expected values. Minimum, maximum, and average values for Mo(V) are 4.87−5.16, with an average = 5.02 units calculated using R_{ij}[Mo(V)] = 1.8790 Å[45] and b = 0.37 Å.[46] Minimum, maximum, and expected values for P(V) are 4.76−5.00, average = 4.90 units, calculated using R_{ij}[P(V)] = 1.604 Å and b = 0.37 Å.[46] Values calculated for individual polyhedra are given in the Supporting Information, Tables S1 (Mo) and S2 (P). Isotropic adp's show a narrow spread with minimum, maximum, and average values for the three atom types of 42 × Mo at 0.0051−0.0062, average = 0.0056 Å^2; 84 × P at 0.0049−0.0068, average = 0.0058 Å^2; and 315 × O at 0.0069−0.0170, average = 0.0097 Å^2.

The driving force for the adoption of this complex superstructure is clearly the need to balance short-range bonding requirements within and between coordination polyhedra with the long-range requirements imposed by its topology. In particular, the $P2_1/c$ subcell structure requires one P−O−P angle to be formally 180° by symmetry. Figure 5e shows the distribution of P−O−P bond angles in the α-$Mo_2P_4O_{15}$

(45) Zocchi, F. *Solid State Sci.* **2000**, *2*, 383–387.
(46) Brese, N. E.; O'Keeffe, M. *Acta Crystallogr., Sect. B* **1991**, *47*, 192–197.

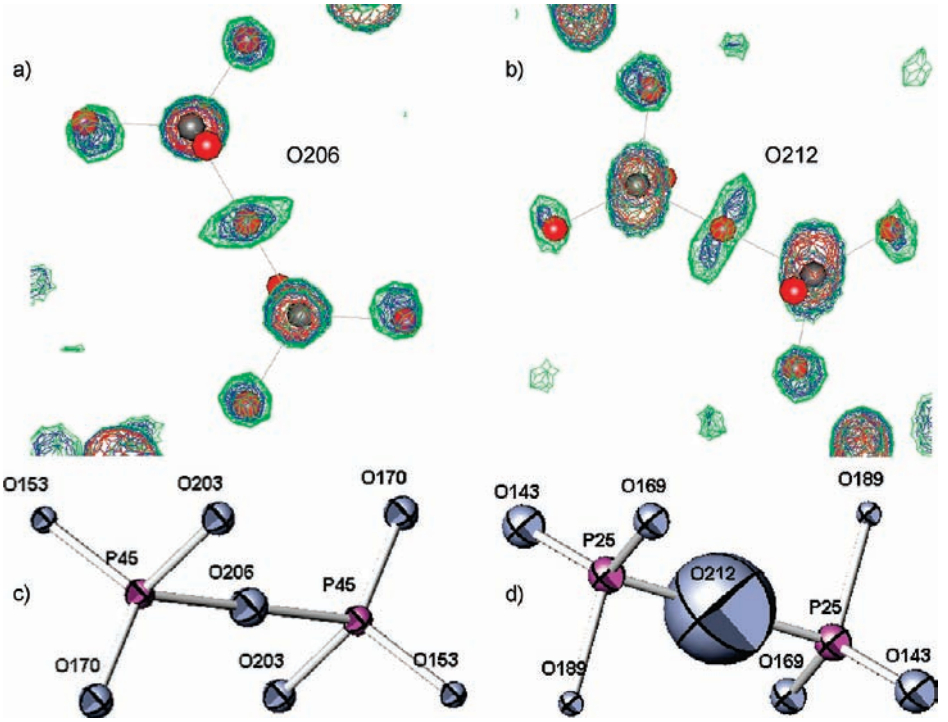

Figure 6. Visual representations of the P_2O_7 units containing O206 and O212. (a,b) Fourier maps drawn using GBR isosurfaces drawn with contours (1) 37, (2) 51, and (3) 95. (c,d) Isotropic displacement parameters drawn at 50% probability.

structure. These angles show an average value of 142°, typical of P_2O_7 groups, though with a relatively wide range of 126–174°. P−O−P angles at the center of a P−O−P−O−P−O−P P_4O_{13} linkage are significantly larger than those at the periphery (average 150 vs 138°). There is also a significant negative correlation between the P−O−P angle and P−O bond length, consistent with increased donation from the lone pair on the bridging oxygen into P−O σ^* bonds as the angle approaches 180° (Figure 7). Importantly, the 174° "outlier" bond angle shown in Figure 5e lies on the general trendline, suggesting that this angle is reliable. Calculations by Birkedal et al. on an isolated $P_2O_7^{4-}$ anion show an equilibrium P−O−P bond angle of 153.4°, which they note is larger than the average bond angle observed experimentally in the 14 crystallographically unique groups of ZrP_2O_7 (145.6°, close to the average observed here).[47] The bending potential is, however, relatively soft, and they calculate a barrier for inversion of P−O−P groups of just 3.6 kJ/mol.

As discussed above and shown in Table 3, there is little or no change in bond distances within coordination polyhedra at high temperatures. For the 24 MoO_6 octahedra in β-$Mo_2P_4O_{15}$, the expected 24:96:24 ratio of short/medium/long bonds is observed, though there is overlap in the distribution in the unrestrained refinement. Data are also consistent with the expected 6:10 ratio of shorter and longer P−O bonds. Central P−O−P angles of P_4O_{13} groups are again higher than peripheral, with average values of 151.2° (assuming O212 has a 137° angle not 180°) versus 141.1°. As might be expected from the volume-increasing ($\Delta V \sim +1\%$) nature of the 523 K phase transition, there is a small increase in average P−O−P angle from 138.4 to 140.3° for peripheral angles and 149.9 to 151.2° for central angles. We note that a local

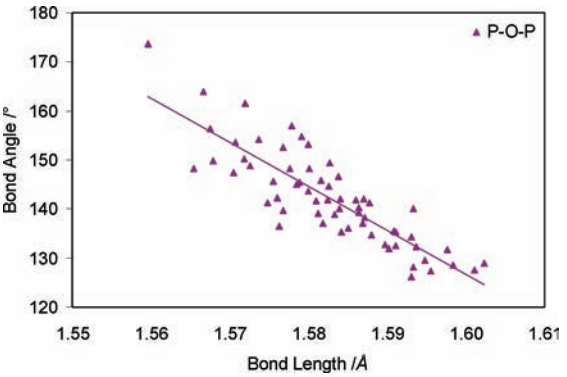

Figure 7. Correlation between P−O bond length and P−O−P bond angles in α-$Mo_2P_4O_{15}$ at 120 K.

increase of P−O−P angle of ~1.7° would cause a P−P distance increase of around 0.5% equivalent to a volume increase of up to ~1.5%.

The relationship between the α and β structures is perhaps revealed most clearly in Figure 8, which compares the $P2_1/c$ subcell model with the true α and β structures. Figure 8a shows "ideal" coordinates in the subcell with the central oxygen of the single unique P_4O_{13} group placed at the $\bar{1}$ site. Figure 8b shows the results obtained by refining this model against experimental data recorded at 120 K using just the reflections predicted by the subcell. As might be expected, the anisotropic displacement parameters (shown here at the 70% level) are large and have shapes/orientations which would be unexpected at low temperatures. Figure 8c shows the true 120 K structure with all sites in the true supercell transformed into a single subcell and displayed with space group symmetry $P2_1/c$. In this representation, each atomic site represents a site in the true supercell. The range of sites therefore indicates the magnitude of shifts of atoms away from average positions

(47) Birkedal, H.; Krogh Andersen, A. M.; Arakcheeva, A.; Chapuis, G.; Norby, P.; Pattison, P. *Inorg. Chem.* **2006**, *45*, 4346–4351.

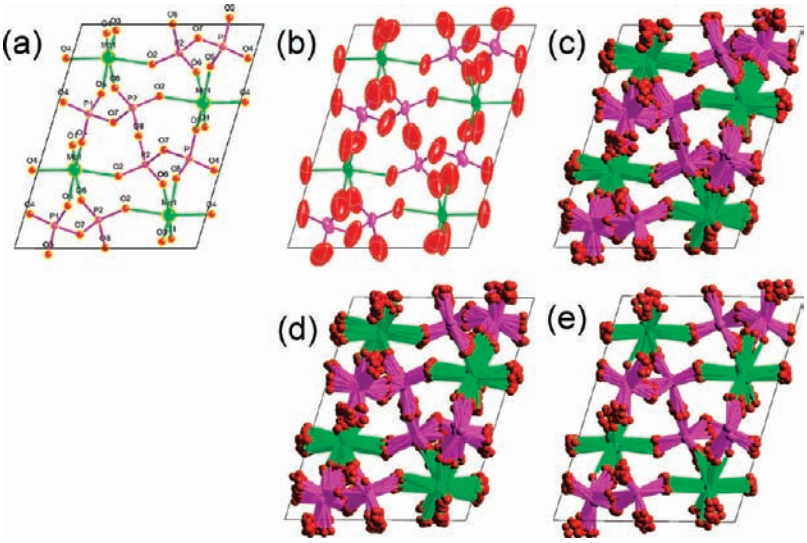

Figure 8. Comparison of the $P2_1/c$, *Pn*, and $P\bar{1}$ structures of $Mo_2P_4O_{15}$ showing all atomic positions in the true superstructure folded into a single unit cell of the $P2_1/c$ model. (a) $P2_1/c$ subcell model, (b) subcell $P2_1/c$ model fitted to 120 K data, (c) 120 K *Pn* model folded into single cell, (d) 293 K *Pn* model folded into single cell, (e) 573 K $P\bar{1}$ model folded into single cell.

and therefore the magnitude of polyhedra displacements and rotations. It is notable that the size and shape of the adp's refined using an incorrect subcell model directly reflect the true pattern of displacements in the supercell—portions of the structure which show small displacement in the low-temperature structure have small adp's and vice versa. It is also clear that oxygen atoms are displaced to a greater extent than Mo and P, which is consistent with the relatively minor changes in X-ray powder data through the phase transition and the observation that X-ray but not neutron powder data fit the subcell model well. Figure 8e shows an equivalent view of the $P\bar{1}$ β structure. From this representation, it is apparent that the distortions from the high-symmetry structure are significantly lower, again consistent with the simplification of the high-temperature neutron powder data.

α- and β-$Mo_2P_4O_{15}$, with 441 and 253 atoms in the asymmetric unit, are complex materials and have the largest and third largest number of atoms in the asymmetric unit reported for crystallographically characterized oxides. It is interesting to examine their complexity relative to other inorganic (using database definitions) materials. One way of doing this is to examine the Inorganic Crystallographic Structural Database (ICSD).[48] This restricts discussion to systems that can be described using 3D space groups (there are then, of course, large families of incommensurate structures omitted), and we omit materials such as the fascinating complex intermetallics related to the Laves phase that have been recently reported.[49] If we accept this approach and take a definition of complexity as being the number of atoms in the asymmetric unit, the vast majority of ICSD entries have a low complexity. As shown by the histogram in Figure 9, of the ~108 000 entries, only ~1000 contain > 100 crystallographically unique atoms and only ~100 more than 250. For the majority of these materials, it is relatively straightforward to identify the origin of their complexity. We discuss this in outline below for all materials with > 100 unique atoms and in more detail for the handful of "non-molecular" structures in this category. Details of the structures discussed are given in the Supporting Information, Table S3.

For commensurate structures, the most obvious origin of structural complexity is chemical complexity: if one has a complex composition or a complex pattern of strong bonds or structure-directing weak interactions in a material, the structure will necessarily be complex. Protein structures fall into this category, as do a large number of recently reported polyoxometallates grown from solution. In the 2008/2 ICSD release, the six most complex (on our limited definition) structures come from Müller and co-workers, with the most complex being $Na_{15}[Mo^{VI}_{126}Mo^{V}_{28}O_{462}H_{14}(H_2O)_{70}]_{0.5}[Mo^{VI}_{124}Mo^{V}_{28}O_{457}H_{14}(H_2O)_{68}]_{0.5}\cdot\sim 400H_2O$ with 937 atoms in the asymmetric unit.[50−55] Looking at the 100 most complex structures, ~85% are polyoxometallates, and a further ~5% have complex compositions containing polyatomic cations or anions and are prepared under nonthermodynamic conditions. The most complex material which we would view as nonmolecular is (for this discussion we categorize the polyoxometallates grown from solution-based species as molecular in nature) $Ba_{45}Cu_{28}Al_{17}F_{197}$ with 574 unique atoms.[56]

A second source of complexity can be associated with materials prepared at high temperatures and which undergo

(48) *ICSD*, v 2008/2; Fachinformationszentrum Karlsruhe and the NIST: Gaithersburg, MD, 2005.

(49) Weber, T.; Dschemuchadse, J.; Kobas, M.; Conrad, M.; Harbrecht, B.; Steurer, W. *Acta Crystallogr., Sect. B* **2009**, *65*, 308–317.

(50) Mueller, A.; Das, S. K.; Fedin, V. P.; Krickemeyer, E.; Beugholt, C.; Boegge, H.; Schmidtmann, M.; Hauptfleisch, B. *Z. Anorg. Allg. Chem.* **1999**, *625*, 1187–1192.

(51) Cronin, L.; Beugholt, C.; Krickemeyer, E.; Schmidtmann, M.; Boegge, H.; Koegerler, P.; Kim, T.; Luong, K.; Mueller, A. *Angew. Chem., Int. Ed. Engl.* **2002**, *41*, 2805–2808.

(52) Mueller, A.; Krickemeyer, E.; Boegge, H.; Schmidtmann, M.; Peters, F.; Menke, C.; Meyer, J. *Angew. Chem., Int. Ed. Engl.* **1997**, *36*, 484–486.

(53) Mueller, A.; Das, S. K.; Fedin, V. P.; Krickemeyer, E.; Beugholt, C.; Boegge, H.; Schmidtmann, M.; Hauptfleisch, B. *Z. Anorg. Allg. Chem.* **1999**, *625*, 1187–1192.

(54) Mueller, A.; Beugholt, C.; Boegge, H.; Schmidtmann, M. *Inorg. Chem.* **2000**, *39*, 3112–3113.

(55) Mueller, A.; Shah, S. Q. N.; Boegge, H.; Schmidtmann, M. *Nature* **1999**, *397*, 48–50.

(56) Dupont, N.; Gredin, P.; Samouel, M.; de Kozak, A. *Z. Anorg. Allg. Chem.* **2002**, *628*, 191–197.

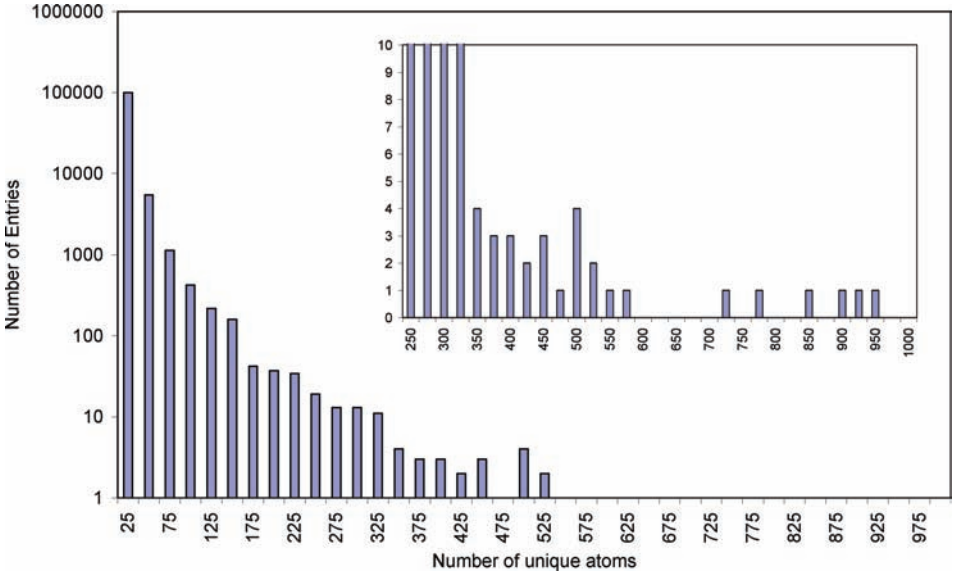

Figure 9. Histogram showing the distribution of entries in the ICSD in 25-atom bins according to the number of atoms in the asymmetric unit. The main plot is presented on a logarithmic scale and the insert on a linear scale.

site ordering on cooling. One such example is α-$La_2Mo_2O_9$ (312 atoms), which, apart from the title phase, is the most complex oxide in the ICSD.[57] At high temperatures (> 580 °C), this material shows high oxide ion conductivity,[58] and its average structure can be described using a cubic cell with just five atoms in the asymmetric unit, though two of these are disordered. When cooling site-ordering of oxide ions occurs, Mo and La adopt a range of local coordination environments, and the room-temperature structure becomes monoclinic with 312 unique atoms. Atom and charge ordering is also the origin of complexity in the 376 atom structure proposed for the perovskite $(Nd_{7/12}Li_{1/4})TiO_3$ by Guiton et al.[59] Here, one must accommodate both Nd/Li A site ordering and phase separation to Nd- and Li-rich regions on a nanometre length scale, which requires a $14a_p \times 28a_p \times 2a_p$ cell (where a_p is the cell parameter of a simple perovskite). Since only transmission electron microscopy and powder data are available on the material, no detailed refinement of the model has been attempted. Similarly, $Sr_4Ga_2O_7$ (104 atoms) can be viewed as a $3 \times 4 \times 4$ perovskite superstructure $[Sr(Sr_{1/3}Ga_{2/3})(O_{7/9}\square_{2/9})_3]$ in which ordering the 22% oxygen vacancies and Ga sites gives rise to a mixture of GaO_4 isolated tetrahedra and Ga_3O_{10} corner-sharing trimers and requires 104 unique atoms.[60] Ordering caused by stereochemically active lone pairs can also lead to complexity, as has been reported for materials such as Bi-containing distorted pyrochlores $Bi_2Sn_2O_7$ and $Bi_2Hf_2O_7$ (both 176 atoms).[61,62] Nowogrocki et al. have reported the structure of $Cs_3B_7O_{12}$ (219 atoms), which has a layered structure containing corner-sharing BO_3 triangles and BO_4 tetrahedra with charge-balancing Cs ions both within and between the slabs.[63] Here, the complexity appears related to achieving stable local coordination environments for all tetrahedral BO_4 and trigonal-planar BO_3 units in the polyanionic network at this particular composition.

Perhaps the most common examples of structural complexity in inorganic materials with simple compositions occur in frameworks based on corner-sharing polyhedra (such as the title compound), which undergo displacive phase transitions on cooling. Common examples where phase transitions lead to a moderate rise in complexity include the quartz and cristobalite polymorphs of SiO_2, perovskites, and WO_3. More complex structures occur for monoclinic and triclinic forms of $AlPO_4$ with tridymite-related structures; by analogy with pure silica polymorphs, these materials are believed to contain 144 and 240 atoms in their asymmetric units at room temperature, though they have only been examined using heavily restrained Rietveld refinements.[64] The most complex frameworks studied by single-crystal methods are ZrP_2O_7 (136 atoms, third most complex oxide)[47] and $Ru(PO_3)_3$ (103 atoms),[65] where the origin of complexity is again due to local bonding requirements of P−O−P linkages. There is also good evidence, for example, from powder diffraction and ^{31}P NMR studies, that related materials such as SnP_2O_7 (540 atoms) are more complex still.[66]

Finally, Kahlenberg et al. have shown how the complex structure of γ-$Na_2Si_2O_5$ (108 atoms) arises from both displacive phase transitions and site ordering.[67] This material has an unusual structure based on Q^3 SiO_4 units that only share three of their four corners with other tetrahedra, such that it is a rare example of an interrupted 3D silicate

(57) Evans, I. R.; Howard, J. A. K.; Evans, J. S. O. *Chem. Mater.* **2005**, *17*, 4074–4077.
(58) Lacorre, P.; Goutenoire, F.; Bohnke, O.; Retoux, R.; Laligant, Y. *Nature* **2000**, *404*, 856–858.
(59) Guiton, B. S.; Hui, Wu; Davies, P. K. *Chem. Mater.* **2008**, *20*, 2860–2862.
(60) Kahlenberg, V.; Lazic, B.; Krivovichev, S. V. *J. Solid State Chem.* **2005**, *178*, 1429–1439.
(61) Evans, I. R.; Howard, J. A. K.; Evans, J. S. O. *J. Mater. Chem.* **2003**, *13*, 2098–2103.
(62) Henderson, S. J.; Shebanova, O.; Hector, A. L.; McMillan, P. F.; Weller, M. T. *Chem. Mater.* **2007**, *19*, 1712–1722.
(63) Nowogrocki, G.; Penin, N.; Touboul, M. *Solid State Sci.* **2003**, *5*, 795–803.
(64) Graetsch, H. *Acta Crystallogr., Sect. C* **2000**, *56*, 401–403.
(65) Imoto, H.; Fukuoka, H.; Tsunesawa, S.; Horiuchi, H.; Amemiya, T.; Koga, N. *Inorg. Chem.* **1997**, *36*, 4172–4181.
(66) Fayon, F.; King, I. J.; Harris, R. K.; Gover, R. K. B.; Evans, J. S. O.; Massiot, D. *Chem. Mater.* **2003**, *15*, 2234–2239.
(67) Kahlenberg, V.; Rakic, S.; Weidenthaler, C. *Z. Kristallogr.* **2003**, *218*, 421–431.

framework and can in fact be viewed as a defect cristobalite network with 20% of the tetrahedral centers removed in an ordered fashion. Above ~560 °C, the material has a relatively simple tetragonal structure which requires, at least on average, one 180° Si−O−Si angle. On cooling, a superstructure with 12 times the volume containing 108 unique atoms forms.

The complexity of $Mo_2P_4O_{15}$ is clearly related to these other framework materials. It is, however, unusual both in the large number of unique atoms at room temperature and since the high-temperature β form retains much of this complexity, requiring 253 atoms in the asymmetric unit and a 6877 Å^3 cell. In fact, the number of free structural parameters per unit volume is barely changed at the α-to-β transition. In the β structure, if both O206 and O212 lie on $\bar{1}$, the number of parameters per subcell unit volume would be 62.75; if O212 is off $\bar{1}$, then that number is 63. In *Pn*, the equivalent number is 63. This contrasts with many frameworks where high-temperature structures are considerably more symmetric than low, though this is not a thermodynamic requirement (for example, systems with re-entrant phase transitions such as Rochelle's salt,[68,69] $Ag_7P_3S_{11}$,[70] and malononitrile[71] involve a high-to-low symmetry transition on warming). In fact, under ambient conditions, $Mo_2P_4O_{15}$ decomposes before it transforms to the expected simple $P2_1/c$ subcell structure. The effective energy barriers for P−O−P inversion within the framework are therefore significantly higher than predicted by simple gas-phase calculations.

Acknowledgment. We thank the EPSRC for funding under EP/C538927/1, STFC for access to ISIS central facilities, and the Royal Society for funding which allowed purchase of the single-crystal high-temperature attachment. SEL thanks Durham University for a Doctoral Training Fellowship. We thank Richard Ibberson and Kevin Knight for assistance with the neutron diffraction experiments. We also thank Bob McMeeking for providing information extracted from the ICSD allowing structures to be ranked according to the number of atoms in their asymmetric unit.

Supporting Information Available: X-ray crystallographic files in CIF format for the $Mo_2P_4O_{15}$ structures at 120, 293, 293 (hothead), and 573 K (hothead), 573 K (restrained) and 653 K (restrained). Tables of low-temperature Mo/P bond valence sum calculations. Table of complex nonmolecular materials in ICSD discussed in the text. This material is available free of charge via the Internet at http://pubs.acs.org.

(68) Beevers, C. A.; Hughes, W. *Proc. R. Soc. London. Ser. A* **1941**, *177*, 251–259.
(69) Suzuki, E.; Shiozaki, Y. *Phys. Rev. B* **1996**, *53*, 5217–5221.
(70) Brinkmann, C.; Eckert, H.; Wilmer, D.; Vogel, M.; auf der Günne, J. S.; Hoffbauer, W.; Rau, F.; Pfitzner, A. *Solid State Sci.* **2004**, *6*, 1077–1088.
(71) Dove, M. T.; Rae, A. I. M. *Faraday Discuss.* **1980**, *69*, 98–106.